A New Radar-Based Statistical Model to Quantify Mass Eruption Rate of Volcanic Plumes

Mereu, Luigi; Scollo, Simona; Garcia, Alexander; Sandri, Laura; Bonadonna, Costanza; Marzano, Frank S.

How to cite

MEREU, Luigi et al. A New Radar-Based Statistical Model to Quantify Mass Eruption Rate of Volcanic Plumes. In: Geophysical research letters, 2023, vol. 50, n° 7, p. e2022GL100596. doi: 10.1029/2022GL100596

This publication URL: https://archive-ouverte.unige.ch//unige:168015

Publication DOI: 10.1029/2022GL100596

AGU ADVANCING EARTH AND SPACE SCIENCE

Geophysical Research Letters®

RESEARCH LETTER
10.1029/2022GL100596

A New Radar-Based Statistical Model to Quantify Mass Eruption Rate of Volcanic Plumes

L. Mereu[1,2], S. Scollo[3], A. Garcia[1], L. Sandri[1], C. Bonadonna[4], and F. S. Marzano[2,5,†]

[1]Istituto Nazionale di Geofisica e Vulcanologia, Sezione di Bologna, Bologna, Italy, [2]CETEMPS Center of Excellence, University of L'Aquila, L'Aquila, Italy, [3]Istituto Nazionale di Geofisica e Vulcanologia, Osservatorio Etneo, Sezione di Catania, Catania, Italy, [4]Department of Earth Sciences, University of Geneva, Geneva, Switzerland, [5]Dipartimento di Ingegneria dell'Informazione (DIET), Sapienza University of Rome, Rome, Italy

†Deceased.

Key Points:

- X-band radar observations of explosive eruptions can be used to estimate the eruption source parameters and associated uncertainties
- Using the Markov Chain Monte Carlo model can be performed the statistical analysis of time series
- Statistical parametric model to infer the mass eruption rate from the measured top plume height

Supporting Information:

Supporting Information may be found in the online version of this article.

Correspondence to:

L. Mereu,
luigi.mereu@ingv.it

Citation:

Mereu, L., Scollo, S., Garcia, A., Sandri, L., Bonadonna, C., & Marzano, F. S. (2023). A new radar-based statistical model to quantify mass eruption rate of volcanic plumes. *Geophysical Research Letters*, *50*, e2022GL100596. https://doi.org/10.1029/2022GL100596

Received 23 SEP 2022
Accepted 24 FEB 2023

Author Contributions:

Conceptualization: L. Mereu, S. Scollo, C. Bonadonna, F. S. Marzano
Data curation: L. Mereu, A. Garcia, L. Sandri
Formal analysis: L. Mereu, S. Scollo
Funding acquisition: S. Scollo, A. Garcia
Investigation: L. Mereu, S. Scollo, F. S. Marzano
Methodology: L. Mereu, L. Sandri, F. S. Marzano

Abstract Accurate forecasting of volcanic particle (tephra) dispersal and fallout requires a reliable estimation of key Eruption Source Parameters (ESPs) such as the Mass Eruption Rate (Q_M). Q_M is usually estimated from the Top Plume Height (H_{TP}) using empirical and analytical models. For the first time, we combine estimates of H_{TP} and Q_M derived from the same sensor (radar) with mean wind velocity values (v_W) for lava-fountain fed tephra plumes associated with 32 paroxysms of Mt. Etna (Italy) to develop a new statistical model based on a Markov Chain Monte Carlo approach for model parameter estimation. This model is especially designed for application to radar data to quickly infer Q_M from observed H_{TP} and v_W, and estimate the associated uncertainty. It can be easily applied and adjusted to data retrieved by radars worldwide, improving our capacity to quickly estimate Q_M and related uncertainties required for the tephra dispersal hazard.

Plain Language Summary New radar-based statistical model useful to quickly infer the mass eruption rate, usually the key parameter to initialize the tephra dispersion model, from the volcanic plume height during the eruptions.

1. Introduction

Tephra injected into the atmosphere during explosive eruptions poses a direct threat to aviation, and when it falls to the ground, it can have widespread primary and secondary impacts at different spatial and temporal scales (e.g., Jenkins et al., 2015). Tephra dispersal and fallout is a function of multiple factors, including Q_M, efficiency of magma fragmentation, clast lithology, vent geometry, H_{TP}, and wind field (e.g., Degruyter & Bonadonna, 2012; Gudmundsson et al., 2012; Mastin et al., 2009; Sparks et al., 1997; Wilson & Walker, 1987). Recent volcanic crises, such as those associated with Eyjafjallajökull (Iceland) in 2010 (Gudmundsson et al., 2012; Mereu et al., 2015), Calbuco (Chile) in 2015 (e.g., Marzano et al., 2018; Romero et al., 2016; Vidal et al., 2017), Etna (Italy) in 2021 (Calvari & Nunnari, 2022) have demonstrated the need of a better real-time assessment of both H_{TP} and Q_M in order to achieve a more accurate tephra dispersal forecasting (Bonadonna et al., 2012; Reckziegel et al., 2016).

Various geophysical strategies for the determination of H_{TP} and Q_M have been developed, such as the data integration from different sensors with field measurement analysis (e.g., Bonadonna et al., 2011; Corradini et al., 2016; Freret-Lorgeril et al., 2021; Mereu et al., 2022; Poret et al., 2018). In fact, the Eruptive Source Parameters can be either based on tephra-fallout deposits (e.g., Carey & Sparks, 1986; Constantinescu et al., 2022; Pyle, 1989; Rossi et al., 2019) or on both ground-based and satellite sensors (e.g., Aiuppa et al., 2015; Dubuisson et al., 2014; Schellenberg et al., 2019; Wood et al., 2019).

It is notable that Q_M has a first-order effect on sedimentation processes that are characterized by different fallout regimes in proximal and distal areas with respect to volcanic vent (e.g., Beckett et al., 2015; Dioguardi et al., 2020; Dürig et al., 2018; Harvey et al., 2018; Scollo et al., 2008). Q_M is typically derived from H_{TP} using models based on the buoyant plume theory (e.g., Bursik, 2001; Carazzo et al., 2008; Degruyter & Bonadonna, 2012; Wilson & Walker, 1987; Woodhouse et al., 2015) or empirical relationship (Mastin et al., 2009; Sparks et al., 1997).

Recently, multi-sensor strategies have been applied with the aim of improving the Q_M estimations (e.g., Freret-Lorgeril et al., 2021; Marzano et al., 2020; Mereu et al., 2020,; Vulpiani et al., 2016). These estimations are often affected by large uncertainties, due to error propagation arising from uncertainties in: (a) H_{TP} estimations,

Project Administration: S. Scollo, A. Garcia
Resources: L. Mereu, S. Scollo, F. S. Marzano
Software: L. Mereu, A. Garcia
Supervision: S. Scollo, A. Garcia, L. Sandri
Validation: L. Mereu, A. Garcia, L. Sandri, C. Bonadonna
Visualization: L. Mereu, A. Garcia
Writing – original draft: L. Mereu
Writing – review & editing: L. Mereu, S. Scollo, A. Garcia, L. Sandri, C. Bonadonna

which are usually based on visible calibrated cameras, radar or satellite retrievals (5%–10%); (b) the assumptions associated with the modeling approach employed (e.g., empirical, analytical); (c) the different definition of H_{TP} retrieved from several sensors; (d) sensors characterized by different size detection limits, operating at various distance from vent and pointing at different regions of volcanic plumes (e.g., Bonadonna et al., 2012). In addition, H_{TP}, as defined in 1D plume models, can differ from the determination of H_{TP} based on various geophysical sensors, especially in case of bent over plumes (e.g., Bonadonna et al., 2012; Scollo et al., 2019). Finally, complex eruptive dynamics (e.g., lava-fountain fed tephra plumes such as those of Etna volcano) cannot be easily described by 1D models designed for sustained eruptions and require dedicated modeling approaches (e.g., Snee et al., 2021).

In this work, we use the data of a weather radar able to scan the Etna summit craters in real time (Vulpiani et al., 2016), to develop a new statistical model for estimating Q_M from H_{TP} and wind velocity v_w observations, accounting for data and modeling uncertainties. This has been possible thanks to a unique data set of fully radar-based pairs of simultaneous and independent Q_M and H_{TP} estimates performed during 32 paroxysms that occurred at Etna between 2011 and 2022.

The paper is structured as follows: Section 2 is devoted to show the radar estimates of H_{TP} and Q_M for the 32 paroxysms; Section 3 describes the model built on such data, and Section 4 summarizes the conclusions.

2. Radar Quantification of Mass Eruption Rate and Top Plume Height

The observations of Etna eruptions are performed by a X-band Weather Radar (XWR), located in Catania, Italy, at about 32 km from the Etna summit. The XWR is a dual-polarization scanning radar, successfully used to retrieve ESPs, which performs a 3-D scan of the surrounding area ∼160 km wide and 20 km tall. XWR can acquire an entire volume moving 360° in azimuth and with 13 fixed angles in elevation with an acquisition time ∼5 min (Mereu et al., 2022; Montopoli, 2016; Vulpiani et al., 2016).

We apply the Volcanic Ash Radar Retrieval (VARR) to the copolar radar reflectivity Z_{hh} (dBZ) with the aim to extract quantitative information of volcanic clouds from radar data (Marzano et al., 2012; Mereu et al., 2015, 2020). In particular we retrieve: (a) the H_{TP} (km) above the Etna summit craters (located at about 3,350 m above sea level), evaluating an uncertainty of ±300 m with respect to the axis of the beam cone, due to scanning radar geometry; (b) the tephra concentration C_t (g/m^3), useful parameter to apply the Mass Continuity Approach (MCA) (e.g., Marzano et al., 2020; Mereu et al., 2015) and quantify the time variation of Q_M (kg/s) (see Supporting Information S1) in the whole radar volume. We identify the most explosive phases of each Etna eruptive activity, named paroxysm, selecting the time when a sustained volcanic plume is formed (Freret-Lorgeril et al., 2018; Scollo et al., 2019). During those events, a rapid transition from Strombolian activity to sustained lava fountains up to a height of a few km is typically observed lasting from 10 min to 1–2 hr (Alparone et al., 2003; Calvari et al., 2018; Snee et al., 2021).

For each paroxysm, we retrieved several pairs of independent Q_M and H_{TP} values, obtaining a set of 242 measurements (Figure 1). The Q_M retrievals range from 10^2 to $5{\cdot}10^6$ kg/s whereas the H_{TP} estimates from 1 to 12 km, including the main variations of Etna explosive activity (Andronico et al., 2021). Although it is known that the radar is not very sensitive to the finest particles (fine ash, smaller 63 μm in diameter) as the sensitivity depends both on the distance between the plume and the radar and on its technical characteristics, it is worth noting that Etna paroxysms are usually characterized by coarser volcanic particles (diameter between 63 μm and 2 mm) has been observed by the deposit analysis (e.g., Andronico et al., 2014; Freret-Lorgeril et al., 2021; Pioli et al., 2019).

Since wind velocity plays a relevant role in the development of the eruption column, we also collected the wind velocity profiles during the 32 paroxysms from the European Centre for Medium-Range Weather Forecasts (ECMWF) ERA5 reanalysis (https://www.ecmwf.int/en/forecasts/datasets/reanalysis-datasets/era5). For each paroxysm, we estimated the mean wind velocity between the Etna summit craters and H_{TP}, which is the parameter v_W used in our statistical model. To quantify an uncertainty in the v_W value, we compared them with wind direction and speed profiles elaborated by a local meteorological model from the hydrometeorological service of ARPA in Emilia Romagna and daily used by Etna volcano observatory to run volcanic ash dispersal forecast (Scollo et al., 2009); the maximum difference between the two estimates is about ±6 m/s that we take as a measure of the uncertainty on v_W.

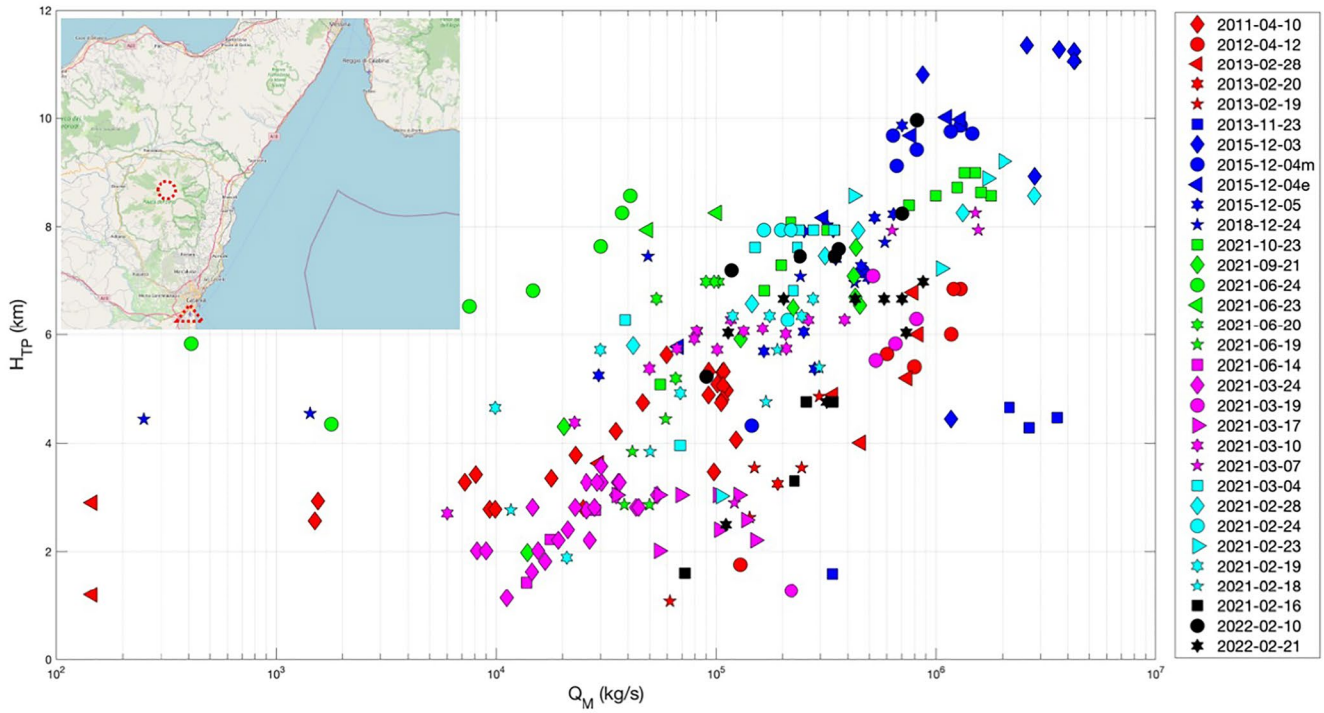

Figure 1. Simultaneous and independent estimates of Q_M (kg/s) and H_{TP} (km) derived from the XWR and related to 32 Etna paroxysms. For each one, the different points, characterized by the same symbol and color, represent the pairs of Q_M and H_{TP} estimated at different times. In the top left, the position of Etna and the XWR are shown in the map with a circle and triangle with a red dotted line, respectively.

3. Model Implementation

Various 1D and 3D models of volcanic plumes exist in literature, all mostly based on the theory of turbulent eruption columns (e.g., Cerminara et al., 2016; Costa & Marti, 2016; Esposti Ongaro et al., 2007; Morton et al., 1956; Oberhuber et al., 1998; Suzuki et al., 2016). In addition, simple empirical models, obtained by different regression analyses between H_{TP} and Q_M of past eruptions have been developed, reflecting the theoretical power law between these parameters (e.g., Aubry et al., 2017; Gudmundsson et al., 2012; Mastin et al., 2009; Sparks et al., 1997). More recently, analytical equations based on the buoyancy theory have been proposed accounting for a variety of eruptive and atmospheric conditions, such as the wind velocity (Degruyter & Bonadonna, 2012; Woodhouse et al., 2015). These are extensively used in practice for quick, near real-time estimations of Q_M from the observed H_{TP} (Folch et al., 2020; Scollo et al., 2019) as well as estimations of Q_M for old deposits (Bonadonna et al., 2015; Pistolesi et al., 2021).

We focus our analysis on the relationship of the Q_M and H_{TP} estimations also considering the effect of v_w and, for the first time, considering only one remote sensing instrument, that is, the radar. This allows to reduce the uncertainty resulting from the combination of multiple remote sensing and modeling strategies associated with different assumptions.

In agreement with the theory of turbulent convection (e.g., Morton et al., 1956; Sparks, 1986; Wilson & Walker, 1987) and consistent with our radar-based measurements, we consider a power law relationship between H_{TP} and Q_M of the form $H_{TP} = \kappa \cdot Q_M^{\gamma}$; fitting this function to Q_M and H_{TP} data sets grouped by similar wind velocities, we have found that while γ remains roughly constant, κ decreases as the wind velocity increases, which is probably an effect of the wind bending the plume (see Supporting Information S1). Considering such evidence, we define a function relating H_{TP} as a function of Q_M and v_W as follows:

$$H_{TP}(Q_M, v_w) = \alpha \cdot e^{\beta \cdot v_w} Q_M^{\gamma} \quad (1)$$

where α, β, and γ are the model parameters to be determined. The inference of the model parameter values is performed using a Markov Chain Monte Carlo (MCMC) method, notably appropriate for solving nonlinear

Table 1
Parameter Values of the α, β, and γ Coefficients of the Model in Equation 1, Inferred Using the Radar-Based Estimates of Q_M and H_{TP} for 31 Eruptions and the v_W Data Retrieved From the ECMWF

Coefficient	Median	16th percentile	84th percentile
α	1.2	0.9	1.7
β	−0.032	−0.038	−0.026
γ	0.16	0.13	0.18

problems and implicitly catching correlations among model parameters (Garcia-Aristizabal, 2018; Garcia-Aristizabal et al., 2016). Markov chains are constructed using the Metropolis-Hastings algorithm (Metropolis & Ulam, 1949; Metropolis et al., 1953); summary statistics of the Markov chains are used to characterize the model parameter values (the median as the best estimation of each parameter, and two percentiles: 16th and 84th are used to define an uncertainty range). We compare the Q_M inferences of our model with those produced by two existing equations:

1. the analytical equation of Degruyter and Bonadonna (2012), hereinafter DB12, considering the v_W parameter:

$$Q_{M-DB12}(t) = a_0 {H_{TP}}^4 + a_1 {H_{TP}}^3 \quad (2)$$

where a_0 and a_1 are coefficients dependent on the gravitational acceleration, air density, buoyancy frequency, top-hat profile radial entrainment coefficient, wind entrainment coefficient, and mean wind velocity profile between vent height and H_{TP} included in a_1 (Degruyter & Bonadonna, 2012; Mereu et al., 2015);

2. the empirical equation of Mastin et al. (2009), hereinafter MA09, expressed by:

$$Q_{M-MA09}(t) = 3.29 \cdot {H_{TP}}^{4.15} \quad (3)$$

assuming a magma density $\rho_m = 2{,}500$ kg/m^3 as prescribed in Mastin et al. (2009).

The inference of the α, β and γ parameters is performed using data from 31 (out of 32) eruptions, since the last eruption in the data set (21 February 2022) is kept aside to be used for testing the model performance. The inferred parameter values (median, 16th, and 84th percentiles) are obtained from the analysis of the MCMC output samples (see Supporting Material) and listed in Table 1.

The solution of $H_{TP}(Q_M, v_w)$ are the surfaces shown in Figure 2. The MCMC samples of α, β, and γ parameters are used to calculate $H_{TP}(Q_M, v_w)$ on a regular grid of Q_M and v_w values; the distribution of H_{TP} values at each grid point are then used to calculate percentiles of interest. We tested the performance model by comparing the Q_M inferred from the H_{TP} observations of 21 February 2022, applying Equation 1, with the Q_M estimated from the XWR measurements for the same event. This event happened during relatively low-intensity wind conditions $v_W \sim 8$ m/s and the model relating Q_M and H_{TP} is shown with black lines in Figure 3.

We note that most of the measurements fall within the represented model's uncertainty bounds, which covers the 68% confidence interval. Two points which are not included correspond to the final phase of paroxysm for which sudden decrease of the eruption column could occur. Figure 3 also shows the curves defined using the DB12 and MA09 models for the parameters characterizing the 21 February 2022 eruption, the first of the two considering the variability $v_w \pm 6$ m/s. It is worth noting that the DB12 model falls within the 68% confidence interval provided by our model for Q_M larger than 6×10^4 kg/s, whereas MA09 for Q_M larger than 2×10^4 kg/s. However, with our model we provide a Q_M range, and not only a single Q_M value, for each H_{TP} single value, that can help the scientist to improve predictions of tephra fallout dispersal and deposit, including the evaluation of associated uncertainty.

In Figure 4, the MCMC samples of the model parameters are used in Equation 1 to obtain a sample of Q_M for each of the H_{TP} values that the radar measured on 21 February 2022. In other words, we show horizontal sections of Figure 3 through the H_{TP} values measured in the testing eruption (red points). During this activity, 12 H_{TP} measurements were retrieved (corresponding to the 12 panels of Figure 4), covering eight different column height values: 1.3, 2.5, 4.8, 4.9, 5.2, 6.0, 6.7, and 7.0 km. Red, blue and green lines show, respectively, the radar-based measurement, the DB12 and MA09 estimate of Q_M for that specific testing point. In panels *a, d, e,* the Q_M estimates (red line) are not shown because they do not belong to the paroxysmal phase. We can note that, of the two red dots outside uncertainty bounds in Figure 3, one Q_M estimate is not captured within the uncertainty bounds shown for our model (Figure 4b), whereas the other Q_M retrieval falls in the upper tail of the histogram (Figure 4c). Moreover, all the estimates of both the DB12 and MA09 models for the testing data fall in the upper tail of the Q_M distribution provided by our model.

4. Conclusion

In this work we present a new parametric model developed and validated on entirely radar-based, simultaneous and independent measurements of Q_M and H_{TP} from 32 Etna paroxysms between 2011 and 2022, also considering

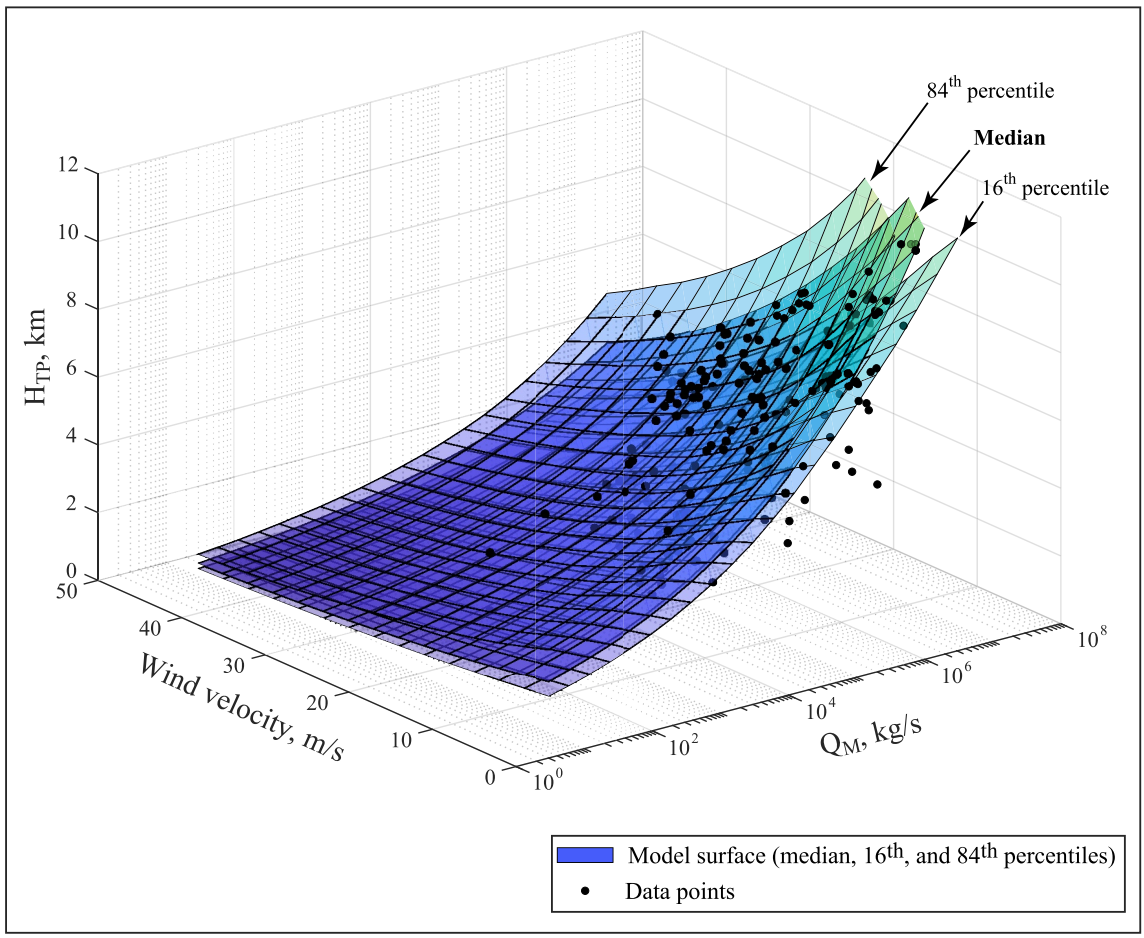

Figure 2. Solutions of the statistical parametric model (Equation 1) shown as surfaces obtained by using the median, the 84th, and the 16th percentiles of H_{TP} values obtained using samples of α, β, and γ obtained from the MCMC method and using a regular grid of Q_M and v_w values. The black dots are the radar-derived samples of H_{TP} and Q_M and the related v_w values from the measurements performed during the 31 Etna eruptions used for fitting the model.

the effect of wind conditions. This calibrated model can be used for near real-time estimation of Q_M during explosive eruptions, given that H_{TP} and v_w measurements are available. We performed the XWR data analysis to estimate pairs of Q_M and H_{TP} during the above-mentioned paroxysms (see Supplementary A) and we extracted the v_w data from the ECMWF ERA5 reanalysis. These simultaneous and independent estimates of Q_M and H_{TP} represent coherent observations of the plume conditions in time-space; this allows increasing the accuracy and consistency of the measurements and, in turn, the accuracy of the model parameters' estimation.

The model is trained on the data from the first 31 eruptive events and tested on the data from the last event, also comparing its performance with those of the DB12 and MA09 models. Most of the testing data falls well within the 68% confidence interval of the calibrated model, except for two data points in Figure 3, one of which is anyway captured within the distribution of sampled Q_M values (Figure 4c), whereas the second is not (Figure 4b). It is notable as all these cases fall within the natural variability of the paroxysmal phase of basaltic volcanoes as Etna (Andronico et al., 2021). Interesting to note that tephra plumes coupled with lava fountains are associated with higher variability of the Q_M-H_{TP} relationship compared to standard plumes (Snee et al., 2021). The DB12 and MA09 models estimates are all consistent with the sampled Q_M values for the testing data; however, the median Q_M from our model is systematically lower than the DB12 and MA09 estimates (Figure 4). Looking at the training data with similar wind conditions as the testing data in Figure 3, we observe that our model captures the variability exhibited by data to a much larger extent ($\backsim$90%) than the DB12 and MA09 models.

Empirical fits are intrinsically dependent on the characteristics of the data set used and typically do not have the capability of an analytical equation to explore and better understand the impact of the different parameters on the

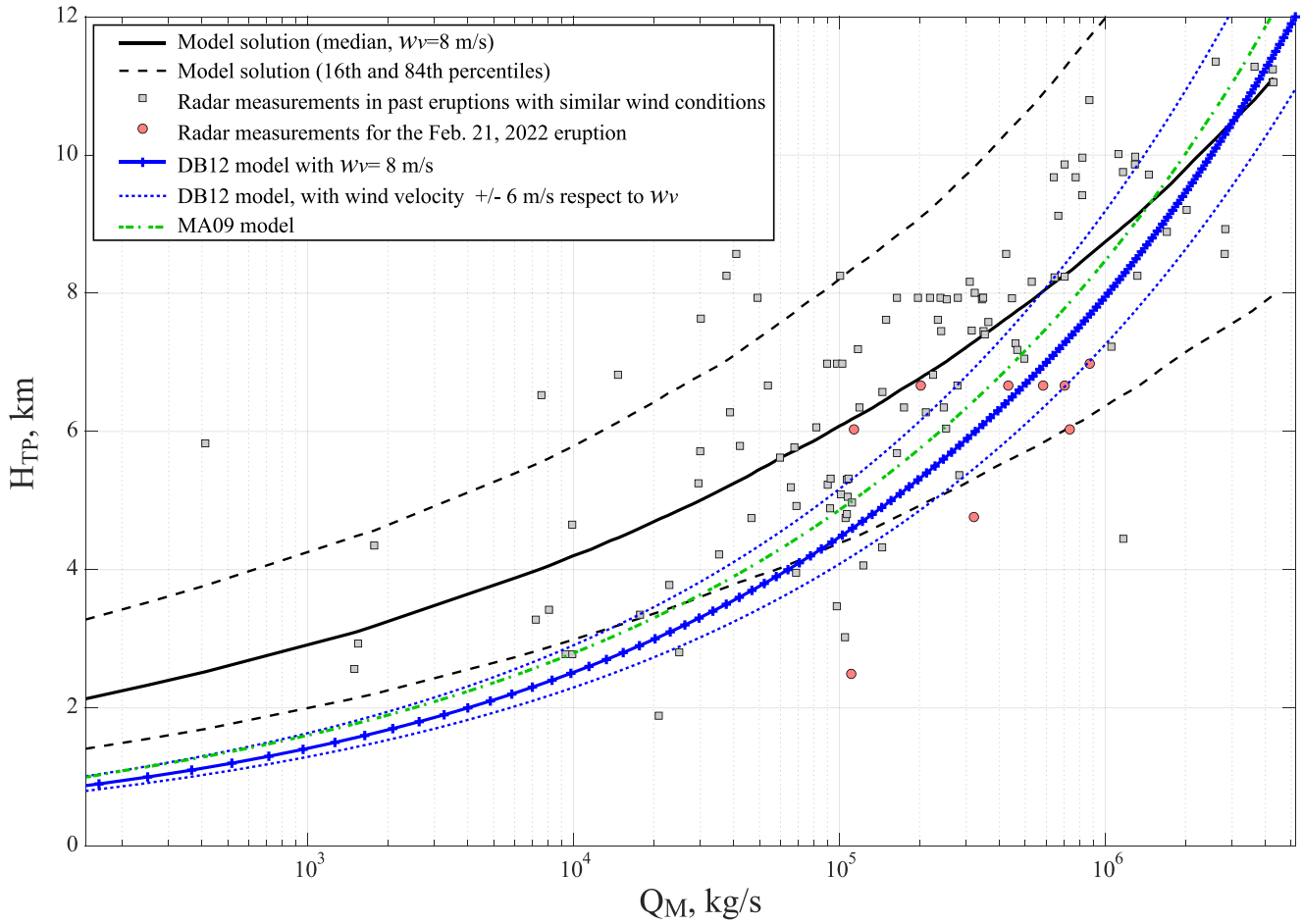

Figure 3. Model relating Q_M and H_{TP} under wind conditions like those observed during the 21 February 2022 eruption ($v_W = 8 \pm 6$ m/s) used for testing (solid black line: median model, dashed black lines: uncertainty defined by the 16th and 84th percentiles). For comparison, the blue lines show the model by DB12 for the same wind conditions, whereas the green line shows the MA09 model. Red points show the estimates of Q_M and H_{TP} for the 21 February 2022 eruption, while the gray squares show the data retrieved from previous eruptive events that happened under similar wind conditions.

results. Nonetheless, our statistical model provides key innovative features: first, it has been entirely developed, for the first time, on self-consistent radar-based H_{TP} and Q_M estimates allowing to eliminate the uncertainty in the definition of parameters; second, being based on lava-fountain fed tephra plumes at Etna, it can better capture the high variability in rise height typical of these plumes. In fact, the MCMC approach is especially appropriate for the description of the Q_M-H_{TP} relation for this eruptive style, which is especially impacted by the combination of various parameters of lava fountains (Snee et al., 2021); Third, it propagates the uncertainty on both the input data (H_{TP} and v_w) and the model parameter values. In this way, uncertainty on Q_M estimates can be propagated and accurately quantified. Although the importance of quantifying uncertainty in volcanic tephra hazard assessment is well known and reported in literature (e.g., Jenkins et al., 2015; Sandri et al., 2016; Selva et al., 2020), real-time forecasting is typically based on deterministic approaches due to technical and operational needs. Accounting for the uncertainty in ESP, among which Q_M is one of the most relevant (Dioguardi et al., 2020; Scollo et al., 2008), would improve the reliability of forecasts and/or short-term hazard assessments of tephra dispersal and fallout (Selva et al., 2014). One of the reasons why deterministic modeling is still the mostly used approach is the need for fast and computationally cheap forecasts during a volcanic crisis, nowadays made possible by the growing availability of computational resources (Martinez Montesinos et al., 2022).

The proposed model, coupled with radar-based real-time measurements of H_{TP} could be easily implemented into the existing short-term tephra dispersal forecasting system of the Etna volcano observatory (Scollo et al., 2019). Moreover, since there are several ground-based radars operating near volcanoes (e.g., Eyjafjallajökull (Mereu et al., 2015) and Grímsvötn (Marzano et al., 2013) in Iceland, Calbuco (Vidal et al., 2017) in Chile, Kelud and

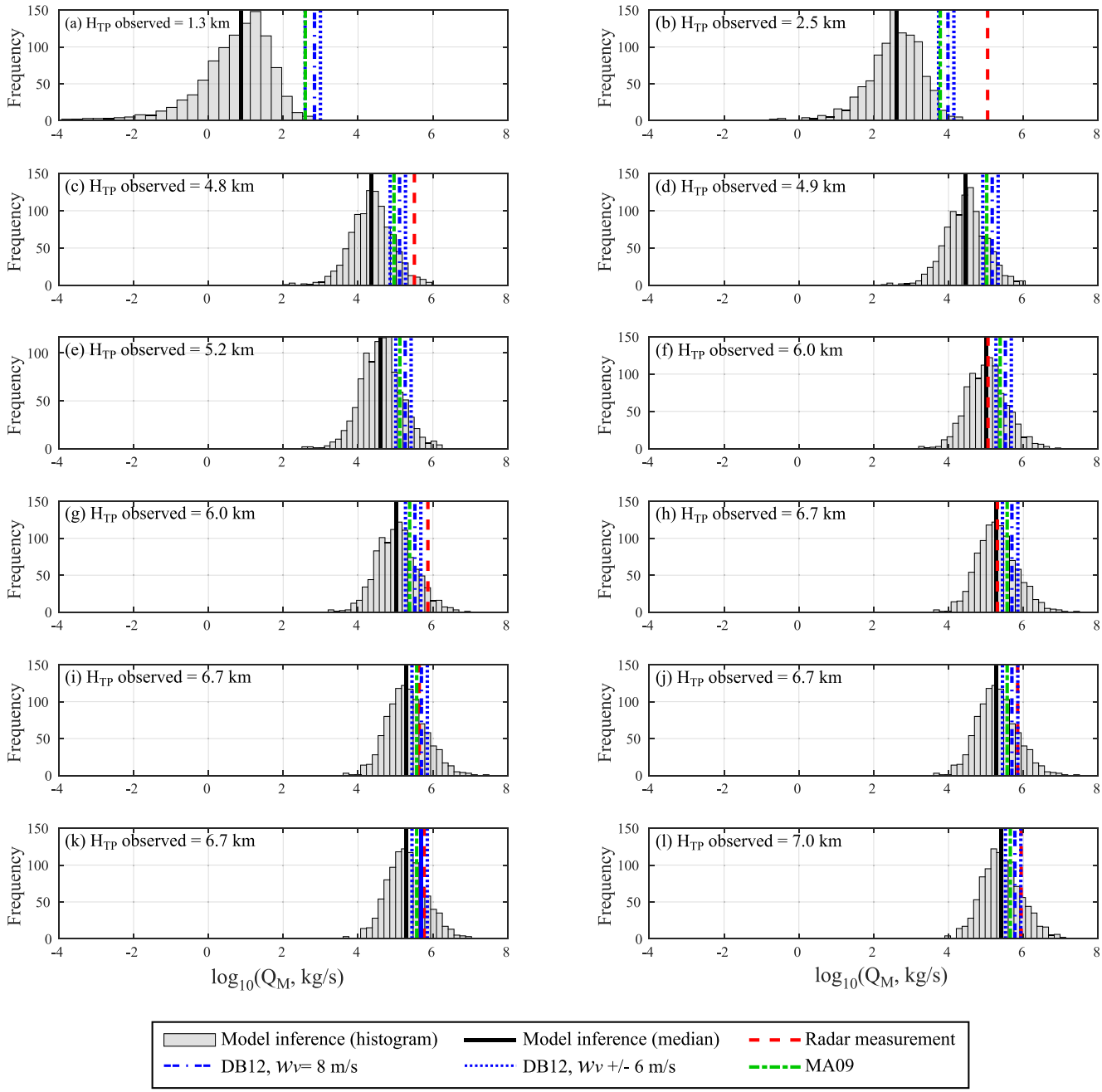

Figure 4. Q_M estimates for the 21 February 2022 testing data according to the proposed model (gray histograms; vertical black lines mark the median), the radar-based measurements (red vertical lines), the DB12 model (blue vertical lines) and the MA09 model (green vertical lines).

Lokon in Indonesia (Wardoyo, 2013)), the adopted approach could be applied to estimate Q_M from radar-based H_{TP} measurements at these volcanoes. Further work using different radar data set of other volcanoes having different eruptive styles is needed to estimate and compare the overall parameters of the statistical model. In this way, we could test both the applicability and limits of the proposed model to quickly quantify the Q_M variability.

Data Availability Statement

The Supplementary A contains a table with the radar retrieval data produced in this work, identified by the acronym RadMER, which has been also released through an open access repository: https://doi.org/10.13127/etna/radmer.

Acknowledgments
The authors would like to thank both the CETEMPS of L'Aquila University, in particular the Eng. Saverio Di Fabio, and the Italian Civil Protection Department (DPC) for the provision of the X-band radar data. This work was performed in the framework of the INGV Project "Pianeta Dinamico" (D53J19000170001), funded by MUR ("Ministero dell'Università e della Ricerca, Fondo finalizzato al rilancio degli investimenti delle amministrazioni centrali dello Stato e allo sviluppo del Paese, legge 145/2018"). The work was also supported by the European project EUROVOLC (European Network of Observatories and Research Infrastructures for Volcanology), funded by the European Union's Horizon 2020 Research and Innovation Programme (Grant 731070).

References

Aiuppa, A., Fiorani, L., Santoro, S., Parracino, S., Nuvoli, M., Chiodini, G., et al. (2015). New ground-based lidar enables volcanic CO_2 flux measurements. *Scientific Reports*, *5*(1), 13614. https://doi.org/10.1038/srep13614

Alparone, S., Andronico, D., Lodato, L., & Sgroi, T. (2003). Relationship between tremor and volcanic activity during the Southeast Crater eruption on Mount Etna in early 2000. *Journal of Geophysical Research*, *108*(B5), 2241. https://doi.org/10.1029/2002JB001866

Andronico, D., Cannata, A., Di Grazia, G., & Ferrari, F. (2021). The 1986–2021 paroxysmal episodes at the summit craters of Mt. Etna: Insights into volcano dynamics and hazard. *Earth-Science Reviews*, *220*, 103686. https://doi.org/10.1016/j.earscirev.2021.103686

Andronico, D., Scollo, S., Cristaldi, A., & Lo Castro, M. D. (2014). Representivity of incompletely sampled fall deposits in estimating eruption source parameters: A test using the 12–13 January 2011 lava fountain deposit from Mt. Etna volcano, Italy. *Bulletin of Volcanology*, *76*(10), 861. https://doi.org/10.1007/s00445-014-0861-3

Aubry, T. J., Carazzo, G., & Jellinek, A. M. (2017). Turbulent entrainment into volcanic plumes: New constraints from laboratory experiments on buoyant jets rising in a stratified crossflow. *Geophysical Research Letters*, *44*(20), 10198–102017. https://doi.org/10.1002/2017GL075069

Beckett, F. M., Witham, C. S., Hort, M. C., Stevenson, J. A., Bonadonna, C., & Millington, S. C. (2015). Sensitivity of dispersion model forecasts of volcanic ash clouds to the physical characteristics of the particles. *Journal of Geophysical Research: Atmospheres*, *120*(22), 11636–11652. https://doi.org/10.1002/2015JD023609

Bonadonna, C., Folch, A., Loughlin, S., & Puempel, H. (2012). Future developments in modelling and monitoring of volcanic ash clouds: Outcomes from the first IAVCEI-WMO workshop on Ash Dispersal Forecast and Civil Aviation. *Bulletin of Volcanology*, *74*, 1–10. https://doi.org/10.1007/s00445-011-0508-6

Bonadonna, C., Genco, R., Gouhier, M., Pistolesi, M., Cioni, R., Alfano, F., et al. (2011). Tephra sedimentation during the 2010 Eyjafjallajökull eruption (Iceland) from deposit, radar, and satellite observations. *Journal of Geophysical Research*, *116*(B12), B12202. https://doi.org/10.1029/2011jb008462

Bonadonna, C., Pistolesi, M., Cioni, R., Degruyter, W., Elissondo, M., & Baumann, V. (2015). Dynamics of wind-affected volcanic plumes: The example of the 2011 Cordón Caulle eruption, Chile. *Journal of Geophysical Research: Solid Earth*, *120*(4), 2242–2261. https://doi.org/10.1002/2014JB011478

Bursik, M. (2001). Effect of wind on the rise height of volcanic plumes. *Geophysical Research Letters*, *28*(18), 3621–3624. https://doi.org/10.1029/2001GL013393

Calvari, S., Cannavò, F., Bonaccorso, A., Spampinato, L., & Pellegrino, A. G. (2018). Paroxysmal explosions, lava fountains and ash plumes at Etna Volcano: Eruptive processes and hazard implications. *Frontiers in Earth Science*, *6*, 107. https://doi.org/10.3389/feart.2018.00107

Calvari, S., & Nunnari, G. (2022). Comparison between automated and manual detection of lava fountains from fixed monitoring thermal cameras at Etna Volcano, Italy. *Remote Sensing*, *14*(10), 2392. https://doi.org/10.3390/rs14102392

Carazzo, G., Kaminski, E., & Tait, S. (2008). On the rise of turbulent plumes: Quantitative effects of variable entrainment for submarine hydrothermal vents, terrestrial and extra-terrestrial explosive volcanism. *Journal of Geophysical Research*, *113*(B9), B09201. https://doi.org/10.1029/2007jb005458

Carey, S., & Sparks, R. S. J. (1986). Quantitative models of the fallout and dispersal of tephra from volcanic eruption columns. *Bulletin of Volcanology*, *48*(2), 109–125. https://doi.org/10.1007/bf01046546

Cerminara, M., Ongaro, T. E., & Neri, A. (2016). Large Eddy Simulation of gas–particle kinematic decoupling and turbulent entrainment in volcanic plumes. *Journal of Volcanology and Geothermal Research*, *326*, 143–171. https://doi.org/10.1016/j.jvolgeores.2016.06.018

Constantinescu, R., White, J. T., Connor, C. B., Hopulele-Gligor, A., Charbonnier, S., Thouret, J. C., et al. (2022). Uncertainty quantification of eruption source parameters estimated from tephra fall deposits. *Geophysical Research Letters*, *49*(6), e2021GL097425. https://doi.org/10.1029/2021GL097425

Corradini, S., Montopoli, M., Guerrieri, L., Ricci, M., Scollo, S., Merucci, L., et al. (2016). A multi-sensor approach for volcanic ash cloud retrieval and eruption characterization: The 23 November 2013 Etna lava fountain. *Remote Sensing*, *8*(1), 58. https://doi.org/10.3390/rs8010058

Costa, A., & Marti, J. (2016). Stress field control during large caldera-forming eruptions. *Frontiers in Earth Science*, *4*, 92. https://doi.org/10.3389/feart.2016.00092

Degruyter, W., & Bonadonna, C. (2012). Improving on mass flow rate estimates of volcanic eruptions. *Geophysical Research Letters*, *39*(16), L16308. https://doi.org/10.1029/2012gl052566

Dioguardi, F., Beckett, F., Dürig, T., & Stevenson, J. A. (2020). The impact of eruption source parameter uncertainties on ash dispersion forecasts during explosive volcanic eruptions. *Journal of Geophysical Research: Atmospheres*, *125*(17), e2020JD032717. https://doi.org/10.1029/2020JD032717

Dubuisson, P., Herbin, H., Minvielle, F., Compiègne, M., Thieuleux, F., Parol, F., & Pelon, J. (2014). Remote sensing of volcanic ash plumes from thermal infrared: A case study analysis from SEVIRI, MODIS and IASI instruments. *Atmospheric Measurement Techniques*, *7*(2), 359–371. https://doi.org/10.5194/amt-7-359-2014

Dürig, T., Gudmundsson, M. T., Dioguardi, F., Woodhouse, M., Björnsson, H., Barsotti, S., et al. (2018). REFIR-A multi-parameter system for near real-time estimates of plume-height and mass eruption rate during explosive eruptions. *Journal of Volcanology and Geothermal Research*, *360*, 61–83. https://doi.org/10.1016/j.jvolgeores.2018.07.003

Esposti Ongaro, T., Cavazzoni, C., Erbacci, G., Neri, A., & Salvetti, M. V. (2007). A parallel multiphase flow code for the 3D simulation of explosive volcanic eruptions. *Parallel Computing*, *33*(7–8), 541–560. https://doi.org/10.1016/j.parco.2007.04.003

Folch, A., Mingari, L., Gutierrez, N., Hanzich, M., Macedonio, G., Costa, A., et al. (2020). FALL3D-8.0: A computational model for atmospheric transport and deposition of particles, aerosols and radionuclides—Part 1: Model physics and numerics. *Geoscientific Model Development*, *13*(3), 1431–1458. https://doi.org/10.5194/gmd-13-1431-2020

Freret-Lorgeril, V., Bonadonna, C., Corradini, S., Donnadieu, F., Guerrieri, L., Lacanna, G., et al. (2021). Examples of multi-sensor determination of eruptive source parameters of explosive events at Mount Etna. *Remote Sensing*, *13*(11), 2097. https://doi.org/10.3390/rs13112097

Freret-Lorgeril, V., Donnadieu, F., Scollo, S., Provost, A., Fréville, P., Guéhenneux, Y., et al. (2018). Mass eruption rates of tephra plumes during the 2011–2015 lava fountain paroxysms at Mt. Etna from Doppler radar retrievals. *Frontiers in Earth Science*, *6*, 73. https://doi.org/10.3389/feart.2018.00073

Garcia-Aristizabal, A. (2018). Modelling fluid-induced seismicity rates associated with fluid injections: Examples related to fracture stimulations in geothermal areas. *Geophysical Journal International*, *215*(1), 471–493. https://doi.org/10.1093/gji/ggy284

Garcia-Aristizabal, A., Caciagli, M., & Selva, J. (2016). Considering uncertainties in the determination of earthquake source parameters from seismic spectra. *Geophysical Journal International*, *207*(2), 691–701. https://doi.org/10.1093/gji/ggw303

Gudmundsson, M. T., Thordarson, T., Höskuldsson, Á., Larsen, G., Björnsson, H., Prata, F. J., et al. (2012). Ash generation and distribution from the April–May 2010 eruption of Eyjafjallajökull, Iceland. *Scientific Reports*, *2*(1), 572. https://doi.org/10.1038/srep00572

Harvey, N. J., Huntley, N., Dacre, H. F., Goldstein, M., Thomson, D., & Webster, H. (2018). Multi-level emulation of a volcanic ash transport and dispersion model to quantify sensitivity to uncertain parameters. *Natural Hazards and Earth System Sciences*, *18*(1), 41–63. https://doi.org/10.5194/nhess-18-41-2018

Jenkins, S. F., Wilson, T., Magill, C., Miller, V., Stewart, C., Blong, R., et al. (2015). Volcanic ash fall hazard and risk. In S. C. Loughlin, S. Sparks, S. K. Brown, S. F. Jenkins, & C. Vye-Brown (Eds.), *Global hazards and risk*. Cambridge University Press.

Martinez Montesinos, B., Titos-Luzón, M., Sandri, L., Rudyy, O., Cheptsov, A., Macedonio, G., et al. (2022). On the feasibility and usefulness of high-performance computing in probabilistic volcanic hazard assessment: An application to tephra hazard from Campi Flegrei. *Frontiers in Earth Science*, *10*, 941789. https://doi.org/10.3389/feart.2022.941789

Marzano, F. S., Corradini, S., Mereu, L., Kylling, A., Montopoli, M., Cimini, D., et al. (2018). Multisatellite multisensor observations of a sub-Plinian volcanic eruption: The 2015 Calbuco explosive event in Chile. *IEEE Transactions on Geoscience and Remote Sensing*, *56*(5), 2597–2612. https://doi.org/10.1109/TGRS.2017.2769003

Marzano, F. S., Lamantea, M., Montopoli, M., Herzog, M., Graf, H., & Cimini, D. (2013). Microwave remote sensing of the 2011 Plinian eruption of the Grímsvötn Icelandic volcano. *Remote Sensing of Environment*, *129*, 168–184. https://doi.org/10.1016/j.rse.2012.11.005

Marzano, F. S., Mereu, L., Scollo, S., Donnadieu, F., & Bonadonna, C. (2020). Tephra mass eruption rate from ground-based X-band and L-band microwave radars during the November 23, 2013 Etna Paroxysm. *IEEE Transactions on Geoscience and Remote Sensing*, *58*(5), 3314–3327. https://doi.org/10.1109/tgrs.2019.2953167

Marzano, F. S., Picciotti, E., Vulpiani, G., & Montopoli, M. (2012). Synthetic signatures of volcanic ash cloud particles from X-band dual-polarization radar. *IEEE Transactions on Geoscience and Remote Sensing*, *50*(1), 193–211. https://doi.org/10.1109/TGRS.2011.2159225

Mastin, L. G., Guffanti, M., Servranckx, R., Webley, P., Barsotti, S., Dean, K., et al. (2009). A multidisciplinary effort to assign realistic source parameters to models of volcanic ash-cloud transport and dispersion during eruptions. *Journal of Volcanology and Geothermal Research*, *186*(1–2), 10–21. https://doi.org/10.1016/j.jvolgeores.2009.01.008

Mereu, L., Marzano, F. S., Montopoli, M., & Bonadonna, C. (2015). Retrieval of tephra size spectra and mass flow rate from C-band radar during the 2010 Eyjafjallajökull eruption, Iceland. *IEEE Transactions on Geoscience and Remote Sensing*, *53*(10), 5644–5660. https://doi.org/10.1109/tgrs.2015.2427032

Mereu, L., Scollo, S., Bonadonna, C., Donnadieu, F., Freret Lorgeril, V., & Marzano, F. S. (2022). Ground-based remote sensing of volcanic mass flow: Retrieval techniques and uncertainty analysis of Mt. Etna eruptions in 2015. *IEEE Journal of Selected Topics in Applied Earth Observations and Remote Sensing*, *15*, 504–518. https://doi.org/10.1109/jstars.2021.3133946

Mereu, L., Scollo, S., Bonadonna, C., Freret-Lorgeril, V., & Marzano, F. S. (2020). Multisensor characterization of the incandescent jet region of lava fountain-fed tephra plumes. *Remote Sensing*, *12*(21), 3629. https://doi.org/10.3390/rs12213629

Metropolis, M., Rosenbluth, A. W., Rosenbluth, M. N., Teller, A. H., & Teller, E. (1953). Equation of state calculations by fast computing machines. *Journal of Chemical Physics*, *21*(6), 1087–1092. https://doi.org/10.1063/1.1699114

Metropolis, M., & Ulam, S. (1949). The Monte Carlo method. *Journal of the American Statistical Association*, *44*(247), 335–341. https://doi.org/10.1080/01621459.1949.10483310

Montopoli, M. (2016). Velocity profiles inside volcanic clouds from three-dimensional scanning microwave dual-polarization Doppler radars. *Journal of Geophysical Research: Atmospheres*, *121*(13), 7881–7900. https://doi.org/10.1002/2015JD023464

Morton, B. B. R., Taylor, G. T., & Turner, J. S. (1956). Turbulent gravitational convection from maintained and instantaneous sources. *Proceedings of the Royal Society of London. Series A. Mathematical and Physical Sciences*, *234*(1196), 1–23.

Oberhuber, J. M., Herzog, M., Graf, H. F., & Schwanke, K. (1998). Volcanic plume simulation on large scales. *Journal of Volcanology and Geothermal Research*, *87*(1–4), 29–53. https://doi.org/10.1016/s0377-0273(98)00099-7

Pioli, L., Bonadonna, C., & Pistolesi, M. (2019). Reliability of total grain-size distribution of tephra deposits. *Scientific Reports*, *9*(1), 10006. https://doi.org/10.1038/s41598-019-46125-8

Pistolesi, M., Aravena, A., Costantini, L., Vigiani, C., Cioni, R., & Bonadonna, C. (2021). Explosive behavior of intermediate magmas: The example of Cotopaxi volcano (Ecuador). *Geochemistry, Geophysics, Geosystems*, *22*(11), e2021GC009991. https://doi.org/10.1029/2021GC009991

Poret, M., Costa, A., Andronico, D., Scollo, S., Gouhier, M., & Cristaldi, A. (2018). Modeling eruption source parameters by integrating field, ground-based, and satellite-based measurements: The case of the 23 February 2013 Etna Paroxysm. *Journal of Geophysical Research: Solid Earth*, *123*(7), 5427–5450. https://doi.org/10.1029/2017jb015163

Pyle, D. M. (1989). The thickness, volume and grainsize of tephra fall deposits. *Bulletin of Volcanology*, *51*, 1–15. https://doi.org/10.1007/bf01086757

Reckziegel, F., Bustos, E., Mingari, L., Báez, W., Villarosa, G., Folch, A., et al. (2016). Forecasting volcanic ash dispersal and coeval resuspension during the April–May 2015 Calbuco eruption. *Journal of Volcanology and Geothermal Research*, *321*, 44–57. https://doi.org/10.1016/j.jvolgeores.2016.04.033

Romero, J. E., Morgavi, D., Arzilli, F., Daga, R., Caselli, A., Reckziegel, F., et al. (2016). Eruption dynamics of the 22–23 April 2015 Calbuco Volcano (Southern Chile): Analyses of tephra fall deposits. *Journal of Volcanology and Geothermal Research*, *317*, 15–29. https://doi.org/10.1016/j.jvolgeores.2016.02.027

Rossi, S., Petrelli, M., Morgavi, D., Vetere, F. P., Almeev, R. R., Astbury, R. L., & Perugini, D. (2019). Role of magma mixing in the pre-eruptive dynamics of the Aeolian islands volcanoes (Southern Tyrrhenian Sea, Italy). *Lithos*, *324*, 165–179. https://doi.org/10.1016/j.lithos.2018.11.004

Sandri, L., Costa, A., Selva, J., Tonini, R., Macedonio, G., Folch, A., & Sulpizio, R. (2016). Beyond eruptive scenarios: Assessing tephra fallout hazard from Neapolitan volcanoes. *Scientific Reports*, *6*(1), 24271. https://doi.org/10.1038/srep24271

Schellenberg, B., Richardson, T., Watson, M., Greatwood, C., Clarke, R., Thomas, R., et al. (2019). Remote sensing and identification of volcanic plumes using fixed-wing UAVs over Volcán de Fuego, Guatemala. *Journal of Field Robotics*, *36*(7), 1192–1211. https://doi.org/10.1002/rob.21896

Scollo, S., Prestifilippo, M., Bonadonna, C., Cioni, R., Corradini, S., Degruyter, W., et al. (2019). Near-real-time tephra fallout assessment at Mt. Etna, Italy. *Remote Sensing*, *11*(24), 2987. https://doi.org/10.3390/rs11242987

Scollo, S., Prestifilippo, M., Spata, G., D'Agostino, M., & Coltelli, M. (2009). Monitoring and forecasting Etna volcanic plumes. *Natural Hazards and Earth System Sciences*, *9*(5), 1573–1585. https://doi.org/10.5194/nhess-9-1573-2009

Scollo, S., Tarantola, S., Bonadonna, C., Coltelli, M., & Saltelli, A. (2008). Sensitivity analysis and uncertainty estimation for tephra dispersal models. *Journal of Geophysical Research*, *113*(B6), B06202. https://doi.org/10.1029/2006jb004864

Selva, J., Bonadonna, C., Branca, S., De Astis, G., Gambino, S., Paonita, A., et al. (2020). Multiple hazards and paths to eruptions: A review of the volcanic system of Vulcano (Aeolian Islands, Italy). *Earth-Science Reviews*, *207*, 103186. https://doi.org/10.1016/j.earscirev.2020.103186

Selva, J., Costa, A., Sandri, L., Macedonio, G., & Marzocchi, W. (2014). Probabilistic short-term volcanic hazard in phases of unrest: A case study for tephra fallout. *Journal of Geophysical Research: Solid Earth*, *119*(12), 8805–8826. https://doi.org/10.1002/2014JB011252

Snee, E., Degruyter, W., Bonadonna, C., Scollo, S., Rossi, E., & Freret-Lorgeril, V. (2021). A model for buoyant tephra plumes coupled to lava fountains with an application to the 29th of August 2011 paroxysmal eruption at Mount Etna, Italy. *Journal of Geophysical Research: Solid Earth*, *126*(12). https://doi.org/10.1029/2020JB021360

Sparks, R. S. J. (1986). The dimensions and dynamics of volcanic eruption columns. *Bulletin of Volcanology*, *48*(1), 3–15. https://doi.org/10.1007/bf01073509

Sparks, R. S. J., Bursik, M. I., Carey, S. N., Gilbert, J. S., Glaze, L., Sigurdsson, H., & Woods, A. W. (1997). *Volcanic plumes* (1st ed.). Wiley.

Suzuki, Y. J., Costa, A., & Koyaguch, T. (2016). On the relationship between eruption intensity and volcanic plume height: Insights from three-dimensional numerical simulations. *Journal of Volcanology and Geothermal Research*, *326*, 120–126. https://doi.org/10.1016/j.jvolgeores.2016.04.016

Vidal, L., Nesbitt, S. W., Salio, P., Farias, C., Nicora, M. G., Osores, M. S., et al. (2017). C-band dual-polarization radar observations of a massive volcanic eruption in South America. *IEEE Journal of Selected Topics in Applied Earth Observations and Remote Sensing*, *10*(3), 960–974. https://doi.org/10.1109/jstars.2016.2640227

Vulpiani, G., Ripepe, M., & Valade, S. (2016). Mass discharge rate retrieval combining weather radar and thermal camera observations. *Journal of Geophysical Research: Solid Earth*, *121*(8), 5679–5695. https://doi.org/10.1002/2016jb013191

Wardoyo, E. (2013). Volcanic ash detection using C-band Doppler radar case study Lokon eruption December 6 2012. In *Paper presented at 1st Asian Conference on Radar Meteorology, Jeju-Korea Selatan*.

Wilson, L., & Walker, G. P. L. (1987). Explosive volcanic eruptions-VI. Ejecta dispersal in Plinian eruptions: The control of eruption conditions and atmospheric properties. *Geophysical Journal of the Royal Astronomical Society*, *89*(2), 657–679. https://doi.org/10.1111/j.1365-246x.1987.tb05186.x

Wood, K., Thomas, H., Watson, M., Calway, A., Richardson, T., Stebel, K., et al. (2019). Measurement of three dimensional volcanic plume properties using multiple ground based infrared cameras. *ISPRS Journal of Photogrammetry and Remote Sensing*, *154*, 163–175. https://doi.org/10.1016/j.isprsjprs.2019.06.002

Woodhouse, M. J., Hogg, A. J., Phillips, J. C., & Rougier, J. C. (2015). Uncertainty analysis of a model of wind-blown volcanic plumes. *Bulletin of Volcanology*, *77*(10), 83. https://doi.org/10.1007/s00445-015-0959-2